4th MASHCON, Hamburg - Uliczka et al. (eds) - © 2016 Bundesanstalt für Wasserbau ISBN 978-3-939230-38-0 (Online)
DOI: 10.18451/978-3-939230-38-0_25

NUMERICAL MODELLING OF PROPELLER-INDUCED FLOW VELOCITIES ON EMBANKMENTS

S Leschka, DHI Deutschland GmbH, Germany
B Xu and **L Yde,** DHI Water & Environment (S) Pte. Ltd., Singapore
O Stoschek, DHI Deutschland GmbH, Germany
J Best, Hamburg Port Authority AöR, Germany

SUMMARY

To support maintenance works of the Bubendey embankment in the Port of Hamburg, DHI set up a computational fluid dynamic (CFD) model to calculate flow velocities on embankments. The model has been calibrated and validated successfully with the help of in-situ measurements, performed by DHI in September 2014. The numerical model is comprised of the exact embankment geometry as well as a parameterized ship propeller. The results have been compared to the results of standard design guidelines [1]. The model leads to lower flow velocities on the embankment compared to available standard methods. It proved its potential in supporting embankment design by leading to less conservative and, thus, more economic design parameters.

1 INTRODUCTION

Ship-induced waves and propeller jets are important loads to be considered for embankment design in ports. Existing design guidelines such as [1] provide empirical formulae which result in high safety values. Flow velocities in a propeller jet for example can be estimated based on simplifying assumptions leading to standardized cases. According to [1], there are four standard cases, which distinguish whether there is a rudder present to split the propeller jet or not and how the dispersion area of the jet is constrained. Here, only vertical quay walls are considered laterally or downstream of the propeller jet.
The estimates are used to determine material characteristics such as rock sizes for safe embankment design. To date, such estimates are on the very conservative side [2]. Increasing ship sizes and thus increasing sizes of bank protection raise the demand of reviewing embankment design methods with the aim to still guarantee safe embankment design but also providing a more economical solution for harbor planners.
Propellers and their interaction with rudders cause complex flow fields in the stern region of a ship. Water is drawn in, accelerated and discharged downstream, propelling the vessel forward. The discharge of water contains high kinetic energy, a turbulent flow and is referred to as propeller jet. The phenomenon comprises velocity components in axial, tangential and radial direction. They can be assessed making use of empirical approaches, physical experiments and numerical modelling.

1.1 EMPIRICAL APPROACHES

Propeller jets have been systematically investigated during the last decades, e.g. in [3] and [4]. [5] describes the flow velocities in the jet with the help of generated thrust, torque and advance velocity of the vessel. The thrust coefficient in particular is dependent on the propeller type [6], which can be parameterized with the help of the pitch ratio H_S/D_p. [7] ascertained K_T for a range between 0.6 and 1.4 and found that the difference of the thrust coefficient is in the order of 100 % for free propellers and even higher for conducted propellers. The velocity distribution in the propeller jet has been described through the axial momentum theory by [3]. The maximum velocity can be calculated according to [8].
The influence of the rudder has been investigated for example in [8], showing that the propeller jet is split into two streams; one is directed upwards to the water surface and the other is directed downwards to the seabed. The maximum jet velocity at the bottom has been described in [9] in dependence of the pitch ratio and a coefficient, which is dependent on whether a rudder is present or not and if the propeller is ducted. Velocity decay with increasing distance and the vertical velocity distribution has been described in [11, 12].

1.2 NUMERICAL MODELLING

In detailed 3-dimensional (3D) numerical modelling (CFD), the following three approaches are often applied to model propeller-induced jets:

- **Sliding Mesh Model**: The computational domain is separated into two domains, a rotor mesh that follows the propeller and a stator mesh that covers the remaining model domain. The sliding grid approach is a transient method where the rotor mesh actually rotates with respect to the stator mesh. The interaction between the rotor and stator are thus fully resolved. This requires a sliding grid interface between the rotor and stator domains to transmit the flow variables across the coupled patches. The sliding mesh approach provides full details of unsteady flow features of propellers.
- **Multiple Reference Frame Approach (MRF)**. Steady-state formulation where the rotor domain

and stator domain are fixed with respect to each other and different reference frames are used in the rotating and stationary parts (momentum equation is modified with Coriolis and centrifugal forces in the rotating reference frame). It allows taking into account the effect of the rotation of the propeller, although no transient rotor-stator interaction is included.

- **Momentum Source Model (MSM)**: Constructed with the purpose of describing the effect of the propeller adequately through a computationally efficient model. The momentum equations include a body-force term which can be used to model the effects of a propeller without resolving the detailed blade flow [13].

The methods have been extensively compared in [14]. The results reveal that propeller characteristics such as the diameter have minor influence on bed velocities compared to parameters such as ship velocity, under keel clearance or rudder angle. Detailed numerical investigations of rudder-propeller interaction showed that as long as the radial variation in axial and tangential momentum generated by the propeller is included, the influence of the unsteady propeller flow can be removed and steady calculations can be performed to evaluate the influence of the propeller on the rudder [15]. Therefore, MSM has been used in this study.

1.3 OUTLINE OF THE STUDY

In this study, the comparison of 3D numerical model results with field measurements is presented for three cases. The measurements are described in section 2. The numerical model setup is given in section 3. This is followed by a result presentation and discussion, setting it into relation with empirical approaches.

2 FIELD MEASUREMENTS

The measurements took place at the Bubendey embankment in Hamburg during one week in September 2014. A sketch of the embankment is given in figure 1.

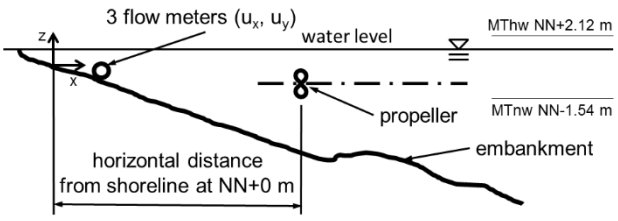

Figure 1. Cross-section of embankment (modified from [16]).

The slope of the embankment was determined to be ~ 1:3 through measurements and surveying. The tug boat "Schleppko" was placed at the embankment in an angle of ~ 90° to the embankment and a pontoon was deployed next to it in order to support the position of the vessel. It features a 500 kW engine. The propeller diameter is 1.72 m. The pitch ratio is 0.661. Figure 2 provides an impression of the scene.

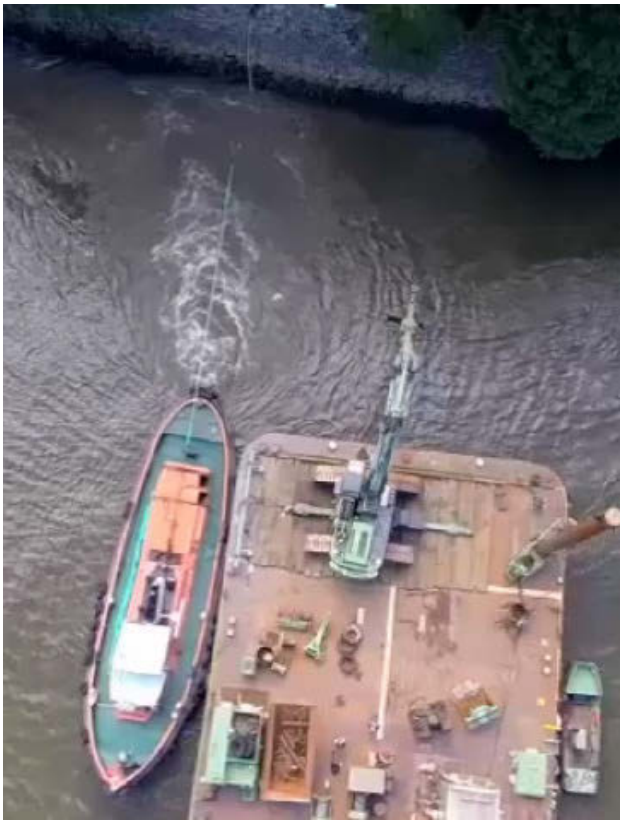

Figure 2. Aerial view of measurements at Bubendey embankment with tug boat "Schleppko" and pontoon.

A slight diversion of the propeller jet towards the left is noted, before the jet enters the shore. It originates from river flow and tide-induced currents. In order to exclude these ambient currents from the measured data, each test was enclosed by two periods of "zero" measurements which took place before and after each test and in which the propeller was not rotating. Thus, the two "zero" measurements only contained the ambient currents. To estimate the magnitude of ambient currents during the period of each propeller test, measurement results have been linearly interpolated over the time between both enclosing "zero" measurements so that the influence of the ambient currents on the propeller test data could be reduced to a large extent.

The measurement conditions considered in this study, including the averaged ambient currents measured at the velocity sensors, are summarized in table 1.

Each propeller test was conducted for a period of three to five minutes.

Scenario 1 has been used to calibrate the numerical model. The scenarios 2 and 3 serve for model validation. 6 velocity sensors have been placed at the propeller axis as well as aside. Three sensors measured the velocity component towards the embankment and three sensors measured the components parallel to the embankment.

The coordinates of the velocity sensors are given in table 2.

Table 1. Measurement conditions.

Scenario	1 Calibration	2 Validation	3 Validation
date	16/9/2014	17/9/2014	19/9/2014
start time	10:56	11:36	0.42
water level [-mNN]	1.42	1.38	1.45
propeller axis level [-mNN]	-0.38	-0.34	-0.32
atmospheric pressure [-hPa]	1019	1019	1012
engine capacity [-%]	50	25	70
rounds/minute [--]	250	192	275
distance from shoreline [-m]	16.55	16.95	16.53
ambient current speed [m/s]	0.16	0.10	0.07

Table 2. Velocity sensor coordinates.

Velocity sensor	x [-m]	y [-m]	z [-mNN]
VS1	1.47	1.80	-0.289
VS2	1.29	-2.19	-0.247
VS3	1.39	-0.06	-0.270

The origin of the coordinate system has been set at the intersection of the shoreline and the propeller axis, when the water level is at NN+0m. The datum NN also provides the vertical reference of the coordinate system (see figure 1).
Figure 3 presents the measured velocities in x direction in sensor VS3, located close to the propeller axis.

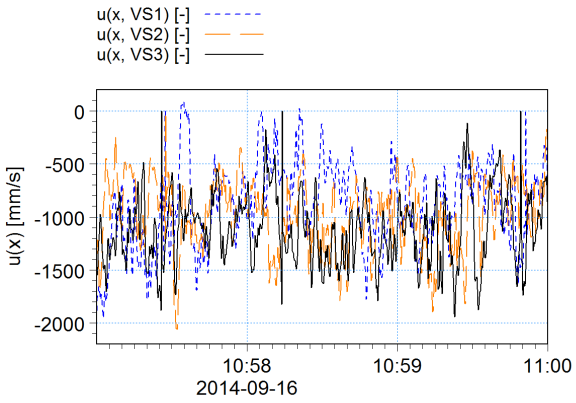

Figure 3. Measured velocity components perpendicular to embankment.

Data reveal high turbulent oscillations, which are in the order of the mean value. This pronounces the importance of considering these fluctuations in further analysis.
While pressures have been measured with 16 pressure sensors distributed along the embankment, the obtained values reveal high sensitivity of the water level fluctuations. The hydrostatic pressures exceeded the dynamic pressures by a factor in the order of 10^2.

3 NUMERICAL SETUP

3.1 OPENFOAM

All CFD simulations are carried out using OpenFOAM ® [17]. CFD simulations have been performed applying the solver simpleFoam. It is based on a steady state Reynolds Average Navier-Stokes (RANS) solver. In a RANS solver, basic equations are averaged and closed by a turbulent closure model that models the effect from turbulence on the mean flow. The result of this approach is that in the momentum equation averaged scales appear as the Reynolds stress tensor. The eddy viscosity hypothesis relates the turbulent stresses to the velocity gradients of the mean flow. The modelling is then reduced to the specification of the eddy or turbulent viscosity (exchange coefficient for momentum) in terms of the local turbulence in the flow.
Preliminary tests showed the importance of the turbulence model in propeller induced flow models. It influences the velocities close to the embankment up to the first order. In this project the k-ε model has been applied. The turbulence quantities k and ε at slope and rudder have been approximated using the corresponding wall functions, whereas zero gradient conditions have been applied at the free flow patches right, left, offshore and top. The turbulence intensity has been estimated to be 10 %, which is in the typical range of high turbulent cases with rotating machinery. The asymmetric body force with axial and tangential components (MSM) was implemented in the numerical solver. The advance coefficient is defined by

$$J = \frac{U_0}{nD_p} \tag{1}$$

where U_0 is the speed of advance, n is the number of propeller revolutions and D_p is the propeller diameter. The thrust coefficient is expressed by

$$C_T = \frac{8K_T}{\pi J^2} \tag{2}$$

with

$$K_T = \frac{T}{\rho n^2 D_p^4}, \tag{3}$$

in which ρ is the water density and T is the thrust. The torque coefficient is expressed by

$$K_Q = \frac{Q}{\rho n^2 D_p^5} \tag{4}$$

with the torque Q. For further details it is referred to [18].

3.2 NUMERICAL DOMAIN AND MESH

The numerical domain and mesh are shown in figure 4.

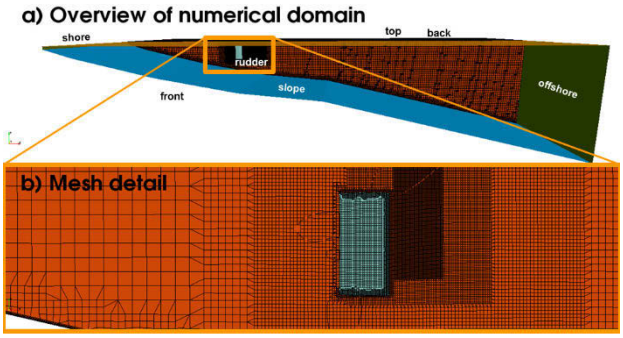

Figure 4. Exemplary computational mesh scene.

The domain extends over 30 m of the embankment length and 43.45 m from the propeller disk into the river. It domain included the exact embankment shape as well as the exact rudder geometry of the tug boat. The ship hull was neglected in the model.

A parametric mesh was created using the snappyHexMesh utility, which forms part of the OpenFOAM ® package. The snappyHexMesh utility generates 3D meshes containing hexahedra (hex) and split-hexahedra (split-hex) automatically from triangulated surface geometries in stereo lithography (STL) format. The mesh has been refined around the rudder and the momentum source field. It approximately conforms to the surface by iteratively refining the intermediate mesh and morphing the resulting split-hex mesh to the surface. The mesh was shrank back from specified surfaces (here from the embankment and the rudder) and additional cells have been inserted resulting in well specified layers. Mesh conversion has been tested by assessing the maximum flow velocity in relation to the cell height at the embankment slope. The deviation between the chosen and the next finer mesh is less than 1 %.The final mesh consisted of approximately 3.0 million cells: The cell height at the embankment slope was 0.01 m.

3.3 BOUNDARY CONDITIONS

The top patch of the numerical domain has been set at the position of the water level. It is noted that the free surface has not been modelled. Thus, the propeller induced water level variations and the rise of water surface close to the shore have been neglected for the sake of simplification and faster model convergence. Thus, slip conditions have been imposed. At the offshore boundary, the so called pressureInletOutletVelocity condition together with the totalPressure condition for pressure have been applied so that water can leave and enter the domain. At the lateral boundaries front and back, the velocity condition inletOutlet has been paired with the fixed pressure value condition. At the bottom, velocities have been set equal to zero and pressures follow the zero gradient condition. In order to account for the sizes of the rocks lying on the embankment slope, the so called nutURoughWallFunction has been applied, allowing incorporating the roughness height of 0.03 m.

3.4 SIMULATION MATRICES

As part of the calibration process, sensitivity tests have been performed, varying the MSM parameters by 10 % each. An overview is given in table 3.

Table 3. Simulation matrix for calibration. The modified values are marked as bold.

scenario	s1.0	s1.1	s1.2	s1.3	s1.4
K_T	0.837	0.837	0.837	0.837	**0.921**
K_Q	0.029	**0.032**	0.029	0.029	0.029
U_0	5.902	5.902	5.902	**6.493**	5.902
J	0.824	0.842	**0.906**	0.842	0.842

The scenarios represent flow fields induced by the tug boat running with 50% of its engine capacity. Scenario s1.0 comprises of original calculated values making use of equations (1) to (4), whereas scenarios 1.1 to 1.4 include the parameter variations. The validation cases are summarized in table 4.

Table 4. Simulation matrix for validation.

scenario	s2	s3
K_T	0.837	0.837
K_Q	0.029	0.029
U_0	5.902	5.902
J	0.824	0.842

In scenario 2, the tug boat runs with 25 % of its engine capacity. In scenario 3, it runs with 70 %.

4 RESULTS

Velocity and pressure data have been analyzed. As total pressure measurements showed high sensitivity to the water level fluctuations during the tests and the CFD model was setup without tracking of the free surface, pressure data has been discarded from the comparisons.
The numerical model calculates averaged values and does not provide information on velocity fluctuations occurring during propeller propulsion. Therefore, the numerically achieved velocities have been compared with averaged measured velocity data. However, as measurements reveal dynamic variations lying in the order of the averaged velocities, they cannot be neglected. In order to maintain the relation between averaged values and fluctuations, the measured fluctuations have been transferred to the numerical results using the relations for the velocities u

$$\frac{u_{i,j,min}}{u_{m1,j,min}} = \frac{u_{i,j,avg}}{u_{m1,j,avg}} = \frac{u_{i,j,max}}{u_{m1,j,max}}. \quad (5)$$

$i = \{1.0, 1.1, 1.2, 1.3, 1.4, 2, 3\}$ indicates the scenario number, $j = \{x, y\}$ the direction of the velocity component, min stands for minimum values, max for maximum values and $m1$ marks measured values during the measurement with 50 % engine capacity. It should be noted that this relation has been adopted for the validation simulations with 25 and 70 % engine capacity, too. x is the direction normal to the embankment (see also figure 1) and y is the parallel direction.

4.1 CALIBRATION

The measured and simulated velocities normal and parallel to the embankment due to a propeller jet caused by the tug boat running with 50 % of its engine capacity are presented in figure 5.

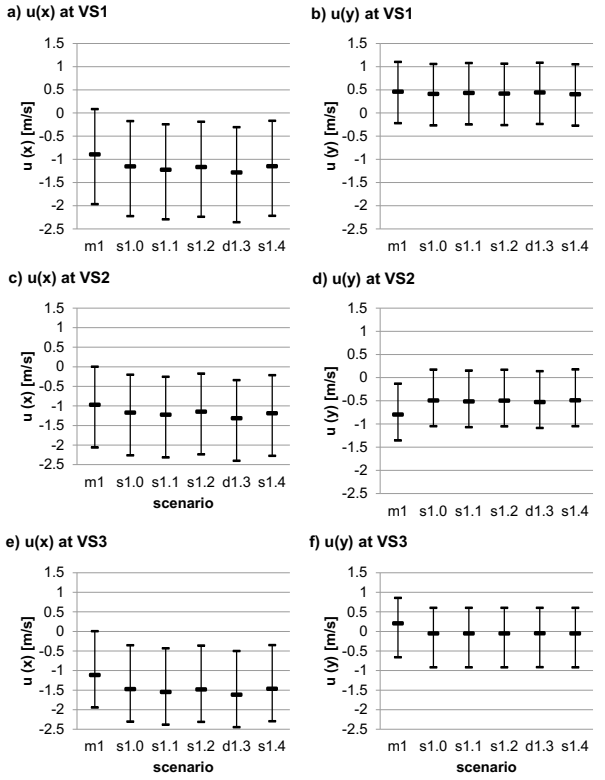

Figure 5. Measured and simulated averaged velocities (calibration with 50 % engine capacity). For m1, the black line spans between the minimum and the maximum measured values, which has been transferred to the simulations s1.0 to s1.4 (see equation (5)).

All numerically achieved velocities exceed the averaged measured velocities towards the embankment (see figures 5.a), c) and e)). The velocity component parallel to the embankment is underestimated (see figures 5.b) and d)), except near the propeller axis (see figure 5.f)). As expected, the velocities are highest near the propeller axis and normal to the embankment. There, the parallel velocity component is comparably small. Scenario s1.3 (increase of U_0) leads to the most conservative results.

Compared to the high fluctuations, the simulated velocities are well within the range of measured velocities. Taking into account these fluctuations and then comparing the maximum velocities normal to the embankment near the propeller axis, the originally derived MSM parameters (scenario s1.0) lead to a deviation of 18 %. The agreement is still good and the numerical model provides results lying on the conservative side. The original parameters of calibration scenario s1.0 have therefore been applied to the validation simulations.

4.2 VALIDATIONS

The calibrated MSM parameter set has been applied to the simulations aiming to reproduce the situations with 25 % and 50 % engine capacities.

4.2 (a) 25 % engine capacity

The measured and simulated velocities normal and parallel to the embankment due to a propeller jet caused by the tug boat running with 25 % of its engine capacity are presented in figure 6.

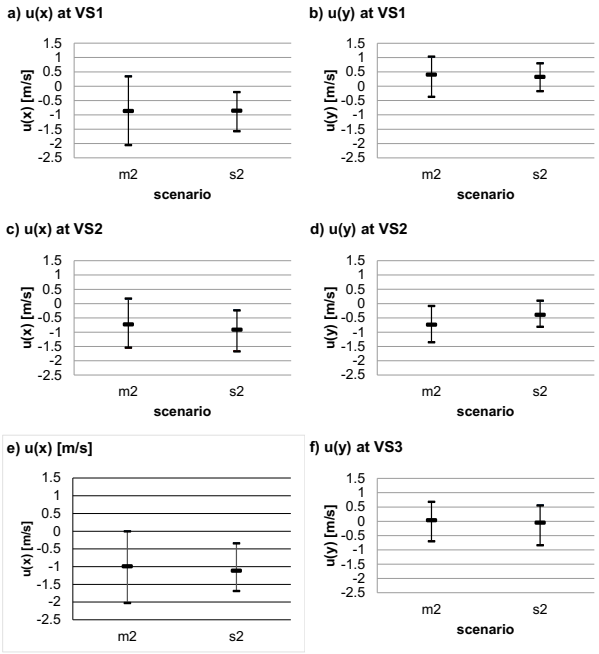

Figure 6. Measured and simulated velocities (validation with 25 % engine capacity). For m2, the black lines span between the minimum and the maximum values. For s2, the black line represents the fluctuation range transferred from the measurement m1 (see equation (5)).

For the velocity component normal to the embankment, the deviation in the outer sensors take values of 1 and 26 % (see figure 6.a) and c), respectively). At the middle sensor, the deviation in maximum velocities is 12 % (see figure 6.e)), whereas the numerically derived value exceeds the measured values. The deviations of the

components parallel to the embankment are slightly higher, especially at the positions of the outer sensors (see figure 6.b) and d)). It can be assumed that the main reason for this deviation lies in the real position of the propeller axis during the measurement. Although the tug boat has been moored at embankment and pontoon, motions could not totally be suppressed. As a consequence, the propeller jet did not hit the embankment at the position of sensor VS3. Nevertheless, the numerical model still provides conservative values.

4.2 (b) 70 % engine capacity

The measured and simulated velocities normal and parallel to the embankment due to a propeller jet caused by the tug boat running with 70 % of its engine capacity are presented in figure 7.

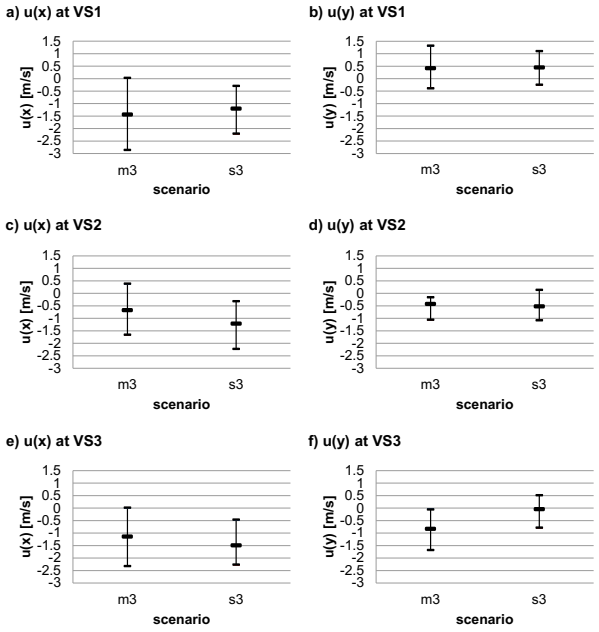

Figure 7. Measured and simulated velocities (validation with 70 % engine capacity). For m2, the black lines span between the minimum and the maximum values. For s2, the black line represents the fluctuation range transferred from the measurement m1 (see equation (5)).

As in the previous comparison (m2 vs. s2), the deviations for velocity components parallel to the embankment are higher than for the components normal to the embankment. This deviation is predominantly governed by the real position of the propeller axis during the measurements. The normal components are underestimated by 17 and overestimated by 81 % (see figure 7.a) and c)), which confirms the observation of the propeller axis. Near the propeller axis, the maximum normal velocities are overestimated by 31 %.
Acceptable agreements for the validation cases have been noted. The numerical model derives conservative values for maximum velocities near the propeller axis in all scenarios.

4.3 COMPARISON WITH GBB STANDARD METHOD

The method considers the propeller parameters diameter D, the factor of applicable propeller rotation rate, the thrust coefficient K_T, design propeller rotation rate and the induced initial velocity U_0. Furthermore, the design pitch ratio H_S/D_p has to be specified. For the here used tug boat, H_S/D_p = 0.661. A differentiation is made between unducted and ducted propellers. Maximum velocities on the embankments are determined based on four standard situations, which are

- **Standard situation 1 (no splitting of the jet)**: Propeller without a middle rudder located behind it; the jet is restricted by the depth of the water but there are no lateral limits to the dispersion of the jet,
- **Standard situation 2 (jet splitting)**: Unducted propeller with a middle rudder located behind it; jet splitting is limited by the depth of the water but no laterally,
- **Standard situation 3 (jet splitting)**: Unducted propeller with a middle rudder located behind it; additional lateral limitation of jet dispersion (by quay wall),
- **Standard situation 4 (no jet splitting)**: Ducted propeller (also with a middle rudder) or unducted propeller without a middle rudder located behind it; dispersion of the jet is limited vertically in the direction of propagation (e.g by a quay wall).

The here investigated situation compares to standard situation 2. The situation is depicted in figure 8.

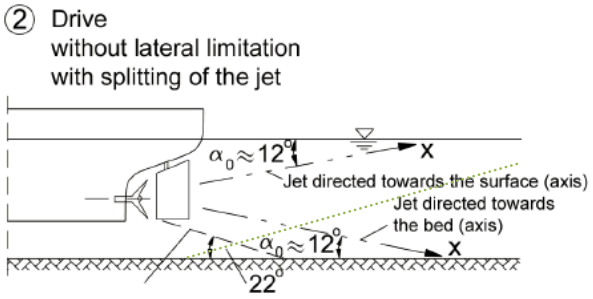

Figure 8. Standard jet dispersion situation 2 (modified from [1]). The green dotted line indicates the idealized slope of the Bubendey quay.

Detailed information on the procedure of determining maximum velocities on the embankment can be taken from [1].

The comparison between CFD and GBB results for all investigated scenarios are given in figure 9.

The velocities have been extracted from the CFD results in a distance of 0.03 m, which is in the range of the equivalent sand grain roughness height [19]. The mean diameter of the rocks on the embankment is 0.1 m. In all cases, the velocities derived with the CFD model fall below the GBB values. The maximum velocities are given in figure 10 and table 4.

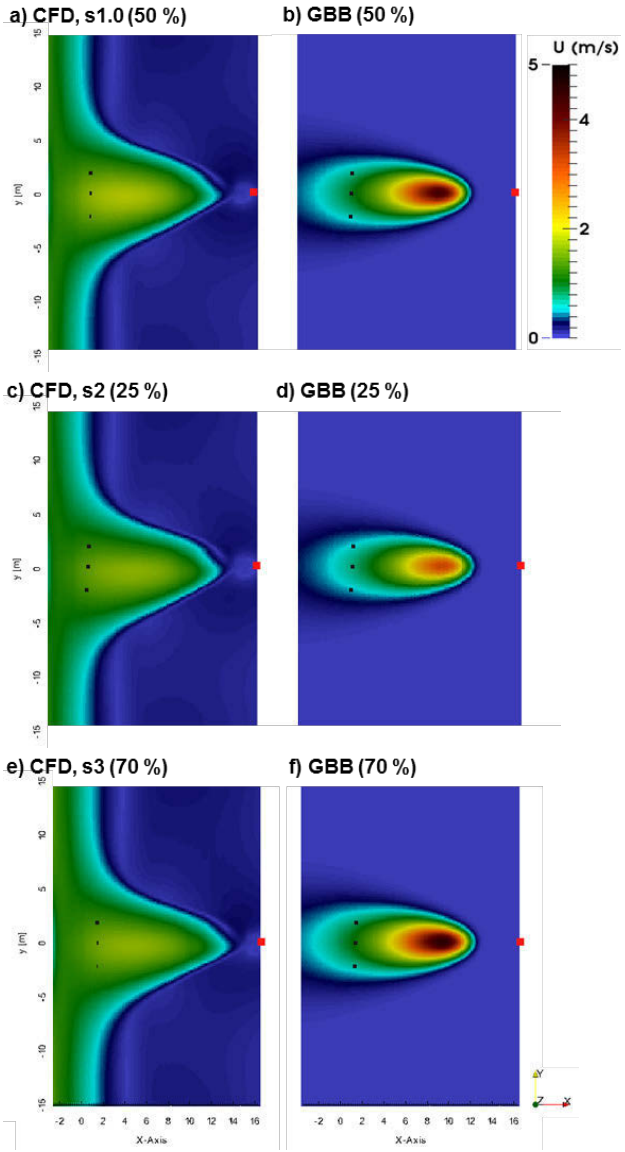

Figure 9. Velocities on the embankment (left: CFD results, right: GBB method) for engine capacities of 25, 50 and 70%. The black dots mark the position of the velocity sensors. The red dot marks the position of the propeller.

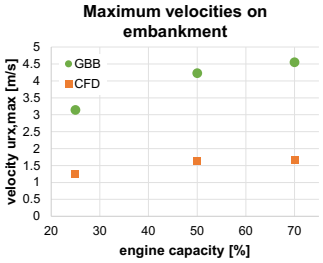

Figure 10. Maximum velocities on embankment after CFD and GBB methods.

Table 4. Maximum velocities on embankment after CFD and GBB methods.

Engine capacity	CFD	GBB
25 %	1.25 m/s	3.14 m/s
50 %	1.63 m/s	4.23 m/s
70 %	1.66 m/s	4.55 m/s

Maximum velocities on the embankment derived by CFD take values between 36 and 40 % smaller than the GBB values. It should be noted that standard situation 2 in [1] considers a horizontal bottom. A slope as found in this application case would deflect the propeller jet upwards. This is not accounted for by the GBB method. When applying the GBB method to a slope as done in this study, the (real) slope is located within the (idealized) undeflected propeller jet, which results in higher velocities. The deviation between CFD and GBB results originates from the high generalization in [1].

5 SUMMARY AND CONCLUSIONS

In this study, a CFD model has been calibrated with the help of in-situ measurements on Bubendey embankment in Hamburg, Germany in September 2014. The model has been validated with the help of two independent data sets originating from the same measurement campaign.
The modelled results are in good agreement with the measurements. It is equally important to point out that the model leads to conservative values.

The results have been compared to the standardized GBB method [1]. For the here tested configurations, CFD results are well below 50 % of the GBB values. The main reason for this deviation originates from the high degree of generalization in the GBB method. For example, the method does not account for the embankment slope. Another reason may have its origin in the measurements used to derive the empirical relations in GBB and to calibrate/validate the CFD model. On one hand, the field measurements comprise of uncertainties, e.g. due to propeller axis orientation during the measurements. From these measurements, mean velocity and its turbulent variation have been obtained. On the other hand, it could not be clarified by the authors if the maximum or the mean value in a propeller jet formed the basis for the GBB standard.

The CFD approach applied in this work has proven to be efficient and economical alternative for embankment design, because it is able to account for local conditions such as embankment slopes.

6 ACKNOWLEDGEMENTS

The authors thank Michel Kopiske (TU Braunschweig) for his contribution regarding the correct application of the GBB method and on measurement data review.

7 REFERENCES

1. BAW (2010). Principles for the Design of bank and Bottom Protection for Inland Waterways, *Bulletin no. 88 of the Federal Waterways Engineering and Research Institute*, Karlsruhe, Germany.

2. PIANC (2015). Guidelines for protecting berthing structures from scour caused by ships, *Report no. 180 of MARCOM WG 48*, Brussels, Belgium.

3. Albertson, M.L.; Dai, Y.B.; Jensen, R.A.; Rouse, H. (1950). Diffusion of a submerged jet. *Transactions of the American Society of Civil Engineers (ASCE)*, (Paper no. 2409) 115: pp. 639-697.

4. Lam, W.; Hamill, G.A.; Song, Y.C.; Robinson, D.J.; Raghunathan, S. (2011). A review of the equations used to predict the velocity distribution within a ship's propeller jet. *Ocean Engineering* 38: pp. 1-10.

5. Steward, D.P.J. (1992). *Characteristics of a ship screw wash and the incluence of a quay wall proximity*. PhD thesis, Queen's University, Belfast/UK.

6. Hamill, G.A.; Johnson, H.T.; Steward, D.P.J. (1995). Estimating the velocity in a ship's propeller Wash. *PIANC Bulletin*, Edinburgh/Scottland, S9.

7. Froehlich, D.C.; Shae, C.C.; Damigella, R.J. (1998). Screwed-Up Riprap: Sizing Rock Riprap to Resist Propeller-Induced Erosion. XII(3). *PB Technote*, PB Network.

8. Blaauw, H.G.; van de Kaa, E.J. (1978). Erosion of bottom and sloping banks caused by the screw race of manoeuvring ships. In *Proc. of the 7th International Harbour Congress* (also Paper no. 202, Delft Hydraulics), Antwerp/Belgium, July 1978.

9. Fuehrer, M.; Roemisch, K. (1977). Effects of modern ship traffic on inland- and ocean waterways and their structures. In *Proc. Of the XXIV. PIANC Congress, Section 1-3*, Leningrad/Soviet Union.

10. Verheij, H.J. (1983). The stability of bottom and banks subject to the velocities in the propeller jet behind ships. *7th International Harbour Congress (also Paper no. 303, Delft Hydraulics)*, Antwerp/Belgium, April 1983.

11. Hamill, G.A.; McGarvey, J.A. (1996). Design for propeller action in harbours. In *Proc. of the 25th International Conference on Coastal Engineering*, Orlando/Florida.

12. Sumer, B.M.; Fredsoe, J. (2002). *The Mechanics of Scour in the Marine Environment*. World Scientific.

13. Hough, G.R.; Ordway, D.E. (1964). The Generalized Actuator Disc. *TAR-TR 6401*, Therm Advanced Research, Inc., Ithaca, New York.

14. DHI (2015). Sediment Re-suspension and Seabed Scour Induced by Ship-Propeller Wash. *Draft Final Report no. 61800151-1*, 18/02/2015, Singapore, Syke/Germany.

15. Phillips, A.; Furlong, M.; Turnock, S.R. (2010). Accurate capture of rudder-propeller interaction using a coupled blade element momentum-RANS approach. *Ship Technology Research (Schiffstechnik)* 57: pp. 128-139.

16. Heinrich Weseloh Straßen- und Tiefbau GmbH (2014). Bubendeyufer Böschungsinstandsetzung Teil 1 Achse 401, *Technical drawing on bottom scanning data 25/07/2014, Station 0+144,000, profile no. 61.3.9*, 9/12/2015.

17. The OpenFOAM Foundation (2011). OpenFOAM-The Open Source CFD Toolbox. *User Guide*, http://www.openfoam.org, last accessed: 23/12/2015.

18. Paterson, E.G.; Wilson, R.V.; Stern, F. (2003). General-purpose parallel unsteady RANS ship hydrodynamics code: CFDSHIP-IOWA. *Report no. 432*, Nov. 2003, IIHR, University of Iowa, Iowa City.

19. Adams, T.; Grant, C.; Watson, H. (2012). A Simple Algorithm to Relate Measured Surface Roughness to Equivalent Sand-grain Roughness. *International Journal of Mechanical Engineering and Mechatronics* 1(1): pp. 66-71.

8 AUTHORS' BIOGRAPHIES

Stefan Leschka holds the position of a senior project engineer and project manager at DHI Deutschland GmbH, Germany. He is responsible for coastal engineering projects on advanced 2D and 3D wave modelling, involving fluid-structure interaction and sediment transport. His previous experience includes wave studies in ports and modelling of floating structures, such as breakwaters and moored ships.

Xu Bin holds the position of a senior CFD engineer at DHI Singapore. He is responsible for developing CFD solutions in relation to these topics including

hydrodynamics, sediment transport and ecological processes in industrial, coastal and marine environments. He is further involved in the development of new CFD technology. His experience includes the analysis of outfall structures, intake structures, etc.

Lars Yde holds the position of the Chief Engineer and is head of the detailed hydrodynamic modelling group in DHI Singapore. He is responsible for all refined hydrodynamic modelling in DHI Singapore. His previous experiences include the modelling of propeller-induced sediment re-suspension.

Oliver Stoschek holds the position if the head of the hydrodynamic and coastal engineering department in DHI Germany. He has focused his work on the studies of currents, scours, sediment transport, thermal re-circulation studies, conceptual design of intake/discharge structures and ship movement in coastal regions as well as coastal protection measures.

Jann Best studied Civil Engineering specialized in Coastal Engineering and Marine Works. Currently, he is Senior Project Manager at the Hamburg Port Authority and responsible for Infrastructure Projects and this Research Project.